

# The scientific payload of the Ultraviolet Transient Astronomy Satellite (ULTRASAT)

Sagi Ben-Ami<sup>1</sup>, Yossi Shvartzvald<sup>a</sup>, Eli Waxman<sup>a</sup>, Udi Netzer<sup>a</sup>, Yoram Yaniv<sup>a</sup>, Viktor M. Algranatti<sup>b</sup>, Avishay Gal-Yam<sup>a</sup>, Ofer Lapid<sup>a</sup>, Eran Ofek<sup>a</sup>, Jeremy Topaz<sup>a</sup>, Iair Arcavi<sup>c</sup>, Arooj Asif<sup>d</sup>, Shlomi Azaria<sup>e</sup>, Eran Bahalul<sup>e</sup>, Merlin F. Barschke<sup>d</sup>, Benjamin Bastian-Querner<sup>d</sup>, David Berge<sup>d,f</sup>, Vlad D. Berlea<sup>d</sup>, Rolf Bühler<sup>d</sup>, Louise Dittmar<sup>d</sup>, Anatoly Gelman<sup>e</sup>, Gianluca Giavitto<sup>d</sup>, Or Guttman<sup>a</sup>, Juan M. Haces Crespo<sup>d</sup>, Daniel Heilbrunn<sup>e</sup>, Arik Kacherginck<sup>e</sup>, Nirmal Kaipachery<sup>d</sup>, Marek Kowalski<sup>d,f</sup>, Shrinivasrao R. Kulkarni<sup>d</sup>, Shashank Kumar<sup>d</sup>, Daniel Küsters<sup>h</sup>, Tuvia Liran<sup>a</sup>, Yonit Miron-Salomon<sup>e</sup>, Zohar Mor<sup>e</sup>, Aharon Nir<sup>e</sup>, Gadi Nitzan<sup>e</sup>, Sebastian Philipp<sup>d</sup>, Andrea Porelli<sup>d</sup>, Ilan Sagiv<sup>e</sup>, Julian Schliwinski<sup>d,f</sup>, Tuvia Sprecher<sup>e</sup>, Nicola De Simone<sup>d</sup>, Nir Stern<sup>e</sup>, Nicholas C. Stone<sup>g</sup>, Benny Trakhtenbrot<sup>c</sup>, Mikhail Vasilev<sup>d</sup>, Jason J. Watson<sup>d</sup>, Steven Worm<sup>d</sup>, and Francesco Zappon<sup>d</sup>

<sup>a</sup>Department of Particle Physics and Astrophysics, Weizmann Institute of Science, Herzl St 234, Rehovot, Israel

<sup>b</sup>Israel Space Agency, Tel Aviv, Israel

<sup>c</sup>School of Physics and Astronomy, Tel Aviv University, Tel Aviv, Israel

<sup>d</sup>Deutsches Elektronen-Synchrotron DESY, Platanenallee 6, 15738 Zeuthen, Germany

<sup>e</sup>ElOp - Elbit Systems Ltd., Rehovot, Israel

<sup>f</sup>Institut für Physik, Humboldt-Universität zu Berlin, Newtonstrasse 15, 12489 Berlin, Germany

<sup>g</sup>Racah Institute of Physics, The Hebrew University, Jerusalem, 91904, Israel

<sup>h</sup>Department of Physics, University of California at Berkeley, 366 LeConte Hall MC 7300, Berkeley, CA, 94720-7300

## ABSTRACT

The Ultraviolet Transient Astronomy Satellite (ULTRASAT) is a space-borne near UV telescope with an unprecedented large field of view (200 deg<sup>2</sup>). The mission, led by the Weizmann Institute of Science and the Israel Space Agency in collaboration with DESY (Helmholtz association, Germany) and NASA (USA), is fully funded and expected to be launched to a geostationary transfer orbit in Q2/Q3 of 2025. With a grasp 300 times larger than GALEX, the most sensitive UV satellite to date, ULTRASAT will revolutionize our understanding of the hot transient universe, as well as of flaring galactic sources. We describe the mission payload, the optical design and the choice of materials allowing us to achieve a point spread function of  $\sim 10$  arcsec across the FoV, and the detector assembly. We detail the mitigation techniques implemented to suppress out-of-band flux and reduce stray light, detector properties including measured quantum efficiency of scout (prototype) detectors, and expected performance (limiting magnitude) for various objects.

**Keywords:** Space-borne telescopes, Ultraviolet, Time domain

## 1. INTRODUCTION

ULTRASAT is a scientific satellite carrying a near UV optimized (NUV; 230 – 290 nm) telescope with an exceptionally wide field of view (FoV) of 200 deg<sup>2</sup>. It is led by the Weizmann Institute of Science and the Israel space agency in collaboration with DESY (Helmholtz association, Germany) and NASA (USA), and planned to

---

Correspondence Author: S.Ben-Ami, sagi.ben-ami@weizmann.ac.il, Telephone: +972-8-9342067

be launched to geostationary transfer orbit (GTO), with operation at geostationary orbit (GEO) commencing at Q2/Q3 2025. The mission is targeting time-domain astrophysics phenomena, and is the first wide FoV telescope operating in the NUV band. For hot sources ( $T \sim 20,000$  K) ULTRASAT is comparable in grasp, the amount of volume of space probed per unit time,<sup>1</sup> to that of the Vera C. Rubin observatory,<sup>2</sup> the largest ground-based optical transient survey planned to begin operation in 2024.

ULTRASAT will undertake the first wide-field UV time-domain sky survey. It will explore a new parameter space in energy (NUV), and time-scale (6 month stares, with a 5-minute continuous cadence). For target of opportunity triggers (ToOs), ULTRASAT will be able to slew in minutes to  $> 50\%$  of the sky. Some of the key scientific questions and phenomena ULTRASAT will target, and in which it is expected to have a significant impact, are:

- The study of gravitational wave sources: The discovery of electro-magnetic emission following the detection of gravitational waves (GW) from the mergers of binaries involving neutron stars.<sup>3,4</sup> Such detections will be the key to using these events for addressing fundamental physics questions, such as the origin of the heaviest elements and the expansion rate of the universe.<sup>5</sup> For GW triggers, ULTRASAT's wide field-of-view amply covers the angular error regions expected to be provided by GW detectors starting 2025.<sup>6</sup> It will provide continuous UV light curves as well as early alerts that will enable ground-based follow-up spectroscopy and monitoring of optical and infrared emission predicted to arise later.
- Early detection of Supernovae: ULTRASAT will collect early UV light curves of hundreds of core-collapse supernovae (CC-SNe) to measure the radii and surface composition of their massive progenitors, as well as to determine explosion parameters.<sup>7</sup> Connecting the pre-explosion stars with their diverse explosive output will chart how the population of massive stars impact their environment through mass loss and explosion, and will specify initial conditions for explosion models.<sup>8-10</sup> Mass loss tracers will further constrain pre-explosion evolution, allowing comprehensive investigation of the final evolution and explosive death of massive stars. During its 3 years mission, ULTRASAT is expected to detect  $> 40$  CC-SNe during the shock breakout phase, and  $> 500$  CC-SNe during the shock cooling phase.
- Determine the high energy flare frequency distribution of stars and guide future exoplanet atmospheric studies: ULTRASAT will monitor  $\sim 10^6$  stars. The long baseline high cadence survey strategy will allow us to characterize UV flares and determine the low frequency - high energy tail of the flaring distribution function, specifically from dM stars, attractive exoplanet hosts for atmospheric characterization due to favorable radii ratio, known to be prodigiously UV flaring stellar objects.<sup>11,12</sup> ULTRASAT will measure, for the first time, the NUV flare frequency and luminosity distribution for stars as functions of both spectral subclass, and stellar rotation period. This will allow the community to assess which stellar types are favored as habitable planet hosts and guide future spectroscopic bio-marker searches with, *e.g.*, JWST and the upcoming ELTs.<sup>13,14</sup>
- Active galactic nuclei: ULTRASAT is poised to provide novel insights into the central engines of Active Galactic Nuclei (AGN), which are powered by accreting supermassive black holes (SMBHs), as the emission from these systems peaks in the UV and is known to vary on essentially all timescales. The study of AGN-related phenomena with ULTRASAT is expected to be broadly split into two regimes. First, ULTRASAT will monitor samples of persistent, vigorously accreting SMBHs over unprecedentedly short timescales, much shorter than the dynamical timescale in the innermost parts of their accretion disks.<sup>15</sup> This will advance our understanding of persistent accretion disks,<sup>16</sup> and may provide new ways to quantify key SMBH properties, such as mass, growth rate, and even spin.<sup>17</sup> Second, ULTRASAT will discover and survey SMBH-related, UV-bright transient phenomena, marking extreme changes to the accretion flows and allowing us to see how SMBHs "turn on" or "off" on exceedingly short timescales,<sup>18,19</sup> and to obtain insights regarding super-Eddington accretion.<sup>20,21</sup>
- Tidal Disruption Events: Stars torn apart in tidal disruption events (TDEs) emit luminous ultraviolet flares.<sup>22-24</sup> ULTRASAT will be able to detect hundreds to thousands of events per year (of which  $\sim 50$  will be at optical magnitudes brighter than 19 and thus easy to follow up from the ground). These discoveries

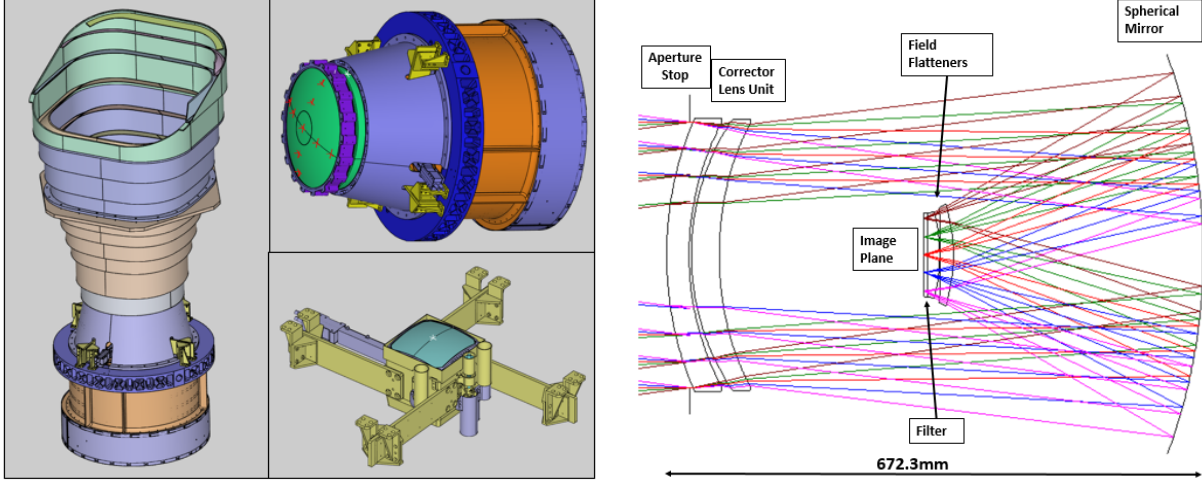


Figure 1: The ULTRASAT payload layout. Left: CAD model of the Payload, the optical tube assembly and the detector assembly; Right: Raytrace layout. The system is a catadioptric one loosely based on a Schmidt design.

will allow us to constrain the currently debated emission mechanisms of TDEs,<sup>25</sup> measure their rates as a function of redshift<sup>26</sup> and probe their peculiar host galaxy preferences.<sup>23,27</sup>

All ULTRASAT data will be transmitted to the ground in real-time, and transient alerts will be distributed to the community in  $< 15$  minutes, driving vigorous ground-based follow-up of static, variable and transient ULTRASAT sources. ULTRASAT is planned for a 3-year operation at a GEO orbit, with fuel sufficient to enable an extension to 6 years of operation. It is planned to reach space prior to the early phase of the planned full sensitivity operation of the GW detector network. In the following paper we describe the ULTRASAT scientific payload design, derived performance, and unique solutions and mitigation techniques adopted for such a unique instrument. The payload prime contractor is EOp - Elbit Systems (Israel), sensors design and manufactured by Analog Value (Israel) and Tower Semiconductors (Israel) respectively, with detector assembly contributed by DESY (Germany) - all managed by the mission program office at the Weizmann Institute of Science in Israel. The spacecraft is developed and manufactured by Israel Aircraft Industries (IAI). An overview of the mission and its science goals will be published in Shvartzvald et al. (in prep.), and further detailed discussion of the payload will be given in future publications by the authors.

## 2. PAYLOAD OVERVIEW

We partition the payload to three parts: Optical tube assembly (OTA), detector assembly (DA) and baffle, see Figure 1 left panel. Each part is described below, with detailed information presented in future publications.

### 2.1 Optical Tube Assembly

The ULTRASAT payload, whose optical layout is shown in Figure 1 right panel, is a wide FoV catadioptric system, loosely based on a Schmidt design.<sup>28</sup> First order parameters are detailed in Table 1. Following a large ( $\sim 800$  mm in length) baffle, the beam is refracted by two aspheric meniscus corrector lenses, a fused silica and a  $\text{CaF}_2$  one, defining the system aperture of 330 mm. While the two substrates are not achromatic pairs in the classical sense at the operation bandpass, the limited choice of high transmission materials in the UV dictates their use as such. The refracted beam is then reflected by a spherical mirror, which delivers most of the optical power of the system. While in a standard Schmidt design, the correctors are placed at the mirror center of curvature, limits on the length of the payload requires us to place the correctors  $\sim 100$  mm closer to the mirror - which is compensated by adding power, 1.136 diopters, to the corrector lenses. The reflected beam is then brought to a focus following refraction by a  $\text{CaF}_2$  and a fused silica field flatteners. The last optical element in front of the detector array is a Sapphire filter with custom coating for out of band suppression, see section 3.2.

Property	Value	Comment
Design	Modified Schmidt	
Number of powered elements	Five	4 refractive, 1 reflective
Aperture	330 mm	
Design Waveband	230 – 290 nm	
Field of View	204 deg <sup>2</sup>	optimized for central 170 deg <sup>2</sup>
Focal length	360 mm	
F/#	1.09	
Plate Scale	0.57 arcsec $\mu\text{m}^{-1}$	
Throughput	Peak $\sim 30\%$	

Table 1: First order parameters of the ULTRASAT telescope.

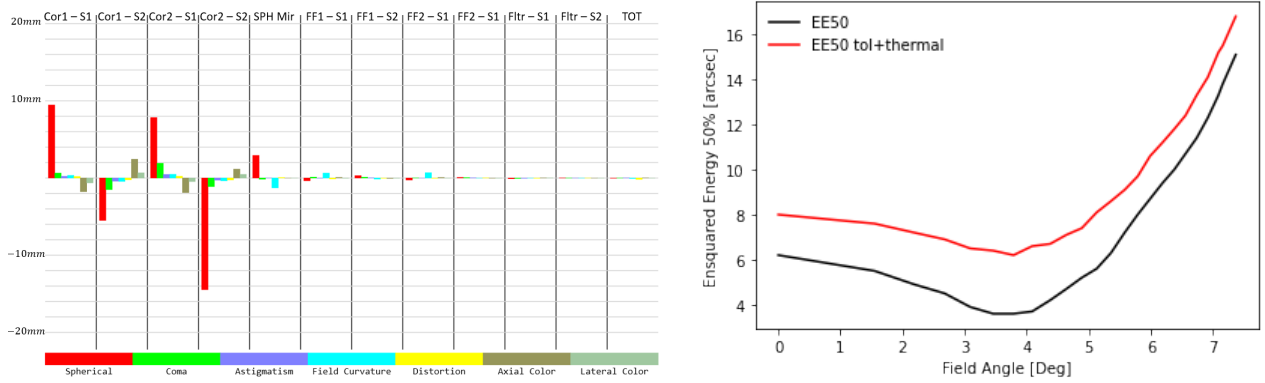


Figure 2: Left: Seidel diagram of the ULTRASAT telescope. Corrector lenses balance spherical aberrations from the mirror, while field curvature is balanced by the two field flatteners; Right: Ensquared energy (50%). Nominal performance are shown in black. Red curve shows expected performance when taking manufacturing and assembly tolerances, as well as thermal gradients on the external corrector and field flattener, into account (90% CL).

The optical design minimizes the Seidel aberrations as shown in Figure 2 left panel, with the corrector lenses canceling 3rd order spherical aberration. The choice of meniscus correctors also allows us to balance aberrations between on-axis and off-axis field points. Field flatteners positioned 5 mm from the focal plane allows us to control field curvature. The nominal 50% mean encapsulated energy diameter (EE50) across the central 170 deg<sup>2</sup> of the FoV is 7.5 arcsec, falling to 10.2 arcsec when taking into account manufacturing and assembly tolerances (90% CL), as well as thermal gradient uncertainties on the external lens - as the telescope is kept at a temperature of  $\sim 21^\circ\text{C}$  while corrector lens is radiating to open space - see Figure 2 right panel. While the former are compensated by serial manufacturing and through a flexible assembly program that allows correction of *e.g.*, element tilt of the field flattener unit, a focus mechanism will compensate for the latter by translating one field flattener lens with respect to the other. The required resolution of the focus mechanism is  $10 \mu\text{m}$ . All optical elements are coated with custom anti reflection coatings (ARC) to minimize Fresnel losses.

## 2.2 Detector Assembly

In the following section we summarise the design of the focal plane array (FPA) and the detector assembly (DA). Further information regarding the detector design can be found in proceeding 12181 – 109 of this volume ('The design of a UV CMOS sensor for the ULTRASAT space telescope', T. Liran et al.) and on an earlier design stage of the DA in a previous publication.<sup>29</sup>

At the heart of the DA is the mosaic assembly comprised of four packaged sensors mounted on a carrier plate, see Figure 3. The sensors are complementary backside illuminated (BSI) metal-oxide-semiconductor (CMOS) devices with 22.4 megapixels and a sensitive area of  $4.5 \times 4.5 \text{ cm}^2$  each. The sensors are passivated using a

Property	Value	Comment
Pixel Type	5T dual gain	Rolling shutter configuration
Pixel scale	5.45 arcsec/pixel	9.5 $\mu$ m pixel with $f = 360mm$ OTA
Wavelength	230 – 290 nm	
Quantum Efficiency	peak > 80%	
Dark Current @ $-73^{\circ}\text{C}$	< 0.026 e/pixel/sec	
Readout Noise	< 3.5 e	

Table 2: Key performance parameters of the ULTRASAT detectors. Further information can be found in proceeding 12181 – 109 of this volume.

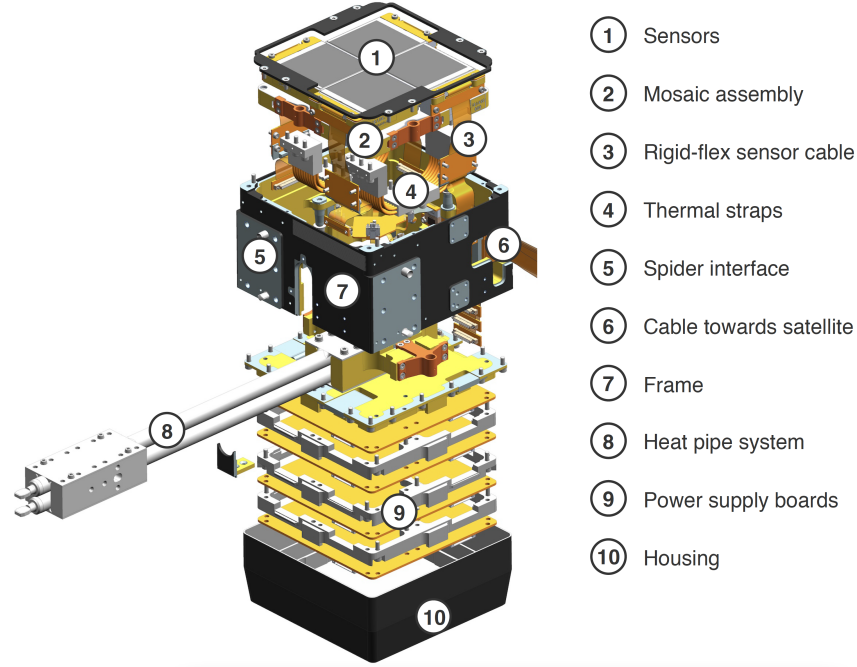


Figure 3: An exploded view of the ULTRASAT focal plane array and detector assembly. The ULTRASAT focal plane is comprised of four CMOS sensors aligned in a windmill configuration. The sensors are back illuminated devices with 22.4 megapixels and a sensitive area of  $4.5 \times 4.5 \text{ cm}^2$  each. The DA houses the sensors and mosaic assembly, thermal interfaces and vicinity electronics boards.

dielectric layer of  $\text{Al}_2\text{O}_3$  with negative fixed charge. High quantum efficiency (QE), average of 59% across the ULTRASAT band with a peak of 80%, is achieved due in part to a custom anti-reflective coating (ARC), taking into account both bandpass and incident angles of rays on the focal plane, see Figure 4 left panel. Main performance parameters are shown in Table 2. The sensors were specifically designed and produced for the ULTRASAT mission by Analog Value Ltd. (AV) and Tower Semiconductor Ltd. (TSL).

The four CMOS sensors are aligned in a windmill configuration. Each sensor is bonded to a CE6 (a controlled expansion alloy of silicon and aluminium) carrier package using an epoxy adhesive, which allows to individually control out-of-plane translation and rotation to make the four tiles of the mosaic co-planar, as a high degree of flatness ( $20\mu\text{m}$ ) is required for such a fast telescope. The sensors are wire bonded to a rigid-flex PCB assembly that additionally carries passive electronic components for noise filtering and connects each sensor to its individual power supply board. The mosaic assembly is thermally isolated from the frame by four flexures made of Ultem to allow for a temperature difference of around 80K between the two elements.

Cooling of the mosaic assembly is realised by a thermal link between the sensor tiles and a thermal interface provided by the spacecraft. It is comprised of four copper rope thermal straps and two propylene heat pipes.

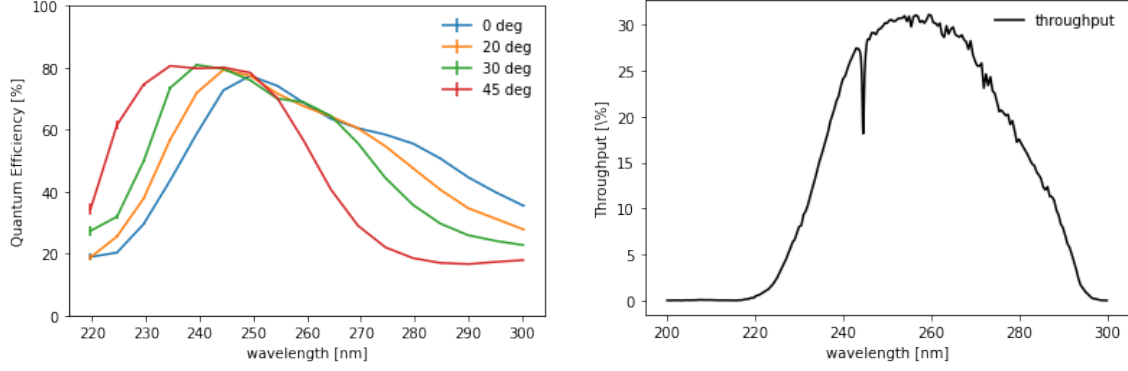


Figure 4: Left: Measured quantum efficiency of a prototype scout sensor with ULTRASAT custom ARC;<sup>30</sup> Right: Overall system efficiency, including optics, detector QE, and geometrical obscuration, averaged across the ULTRASAT FoV.

Each thermal strap is connected to one of the sensor tiles to mechanically decouple the mosaic from the heat pipes. Temperature control of the sensors is performed by the spacecraft’s on-board computer with the help of heaters located on the sensor tiles. To achieve the higher temperatures required for decontamination of the sensors additional heaters are placed along the spacecraft’s side of the thermal chain.

The DA’s structural design is based on a milled frame, which ensures mechanical integrity and thus low displacements when being loaded mechanically or thermally. The frame is machined from titanium and provides the mechanical interfaces towards four “spiders” that connect the DA to the telescope. Furthermore, the frame provides the mechanical interfaces to a Sapphire filter window placed  $550\mu\text{m}$  above the sensors and a motorised focus mechanism that is attached at the side of the DA and allows for adjustments of the distance between first field flattener in the optical train and the mirror. The frame also provides interfaces to the interior of the DA, where the mosaic assembly, as well as the heat pipe system are attached. At the back of the frame a PCB stack accommodating the high precision power supplies for the sensors is located. An exploded view of the DA’s interior is shown in Figure 3.

### 2.3 Baffle

A large baffle is placed in front of the telescope aperture stop. It is designed to suppress stray light into the OTA, as well as reduce the electron flux on the external corrector plane. It is fabricated from 4.2 mm thick aluminum sheets, and its interior is coated with Acktar vacuum black. At the edge of the baffle, a trap door is located to shield and protect the OTA during launch and transit to GEO. The Baffle is shown in Figure 5. Further information can be found in section 3.3.

## 3. UNIQUE CHALLENGES AND MITIGATION STRATEGIES

### 3.1 Radiation Environment and Cherenkov Radiation Background

The harsh environment at GEO entails a significant radiation flux intercepting the OTA, specifically the front corrector lens\*. While the substrate of the corrector lens is Corning HPF7980, a high purity synthetic fused silica with high transmission in the UV, radiation damage is known to create absorption centers, specifically in the UV, due to *e.g.*, compactness, and generation of vacancies in the crystal structure. We therefore embarked on a dedicated campaign to both simulate the radiation environment on critical elements in the OTA and to measure the induced absorption at such levels.

Simulation of the radiation environment was performed by RASL (UK) based on the IGE2006 model. The external corrector outer surface receives a total ionising dose (TID) of  $10^5$  Krads per year, dominated by trapped

\*Radiation hardening of the detector is discussed in proceedings 12181 – 109 of this volume, ‘The design of a UV CMOS sensor for the ULTRASAT space telescope’, T. Liran et al.



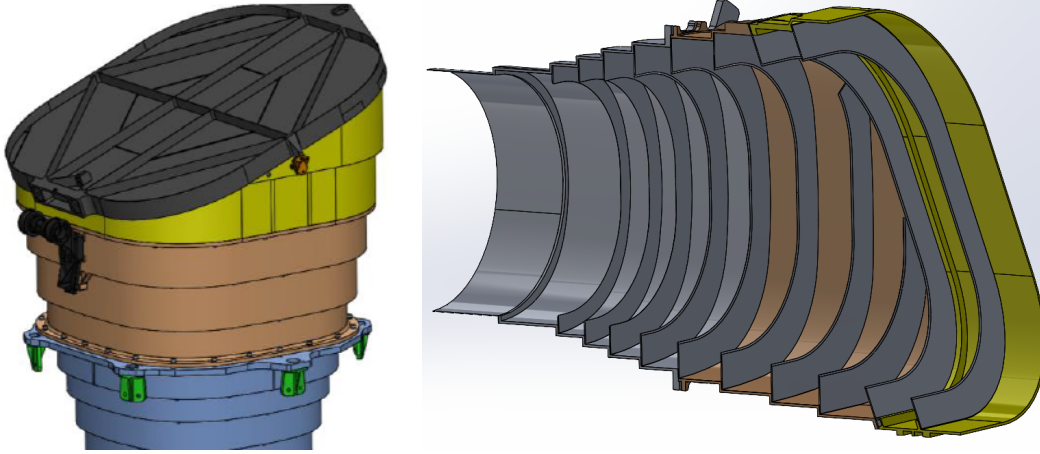


Figure 5: Left: ULTRASAT baffle with the protective trap door closed; Right: A cross section of the baffle showing internal vane structure. The inside is coated with Acktar vacuum black.

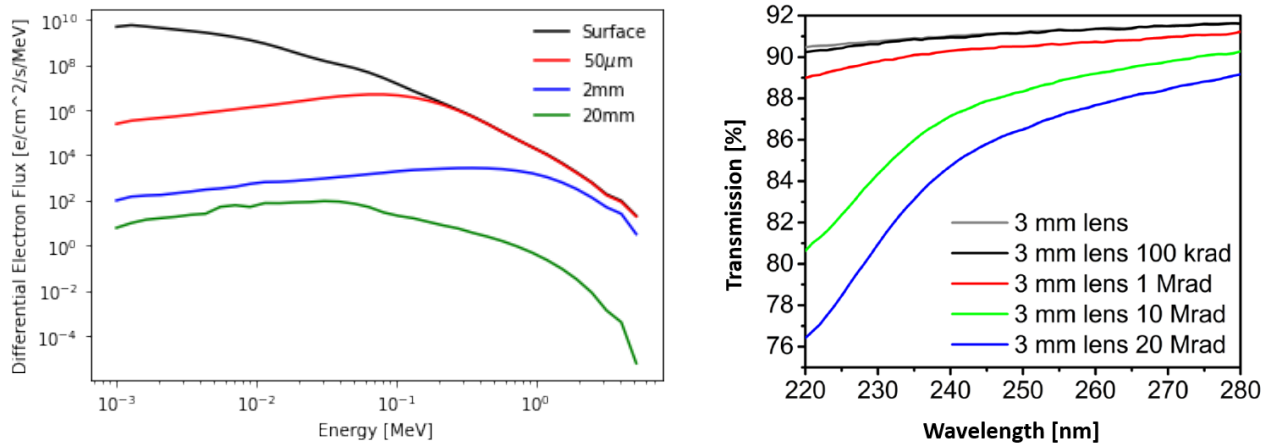


Figure 6: Left: Simulated radiation level in the external corrector lens; Right: Transmission of witness samples of Corning HPF7980 before and after radiation, not corrected for Fresnel losses. We use these results to extrapolate, taking into account the difference in penetration length between the gamma radiation (<sup>60</sup>Co) and energetic electrons (in orbit), to conclude an estimated transmission loss of < 2% in a period of 3 years, and only at wavelengths shorter than ~ 245 nm.

electrons in the orbit. The electron flux drops rapidly deeper into the lens, with an order of magnitude drop for electrons with energies of ~ 0.1 MeV at a depth of ~ 50μm, see Figure 6 left panel. The expected electron dose above 0.1 MeV, the threshold for dislocations in the lattice, at the corrector surface is ~ 10 Mrad/yr, due in part to significant attenuation by the baffle.

We then turned to measure UV transmission of the substrate samples at such radiation levels. Several samples of Corning HPF7980 were radiated using a <sup>60</sup>Co source, for a total integrated radiation of up to 20 Mrad at Soreq NRC in Israel. UV transmission was measured before and after the samples were exposed to the radiation source using a dedicated setup and a monochromator. The results, see Figure 6 right panel, were then extrapolated to ULTRASAT based on the radiation analysis described above, and taking into account the different penetration depth of electrons and gamma radiation, the former being the dominant factor on orbit while the latter being the dominant factor for the <sup>60</sup>Co source. We conclude expected transmission deterioration of < 2% in a period of 3 years, and only at wavelengths shorter than ~ 245 nm.

The catadioptric design of the OTA, with refractive lenses at the front, raises another challenge due to Cherenkov radiation resulting from relativistic electrons propagating at velocities faster than the phase velocity in the substrate. This emission is predominantly in the UV, and will result in lower contrast and visibility in ULTRASAT images, similar effect to that of pupil ghosts. The baffle was designed to significantly reduce the electron flux on the corrector, and we find an estimated contribution of  $0.1 \text{ photons s}^{-1}$  per pixel, which will result in noise contribution similar to that of the detector readout noise for integration time of 300 sec, and lower than the noise expected from zodiacal light, see section 3.3.

### 3.2 Out-of-Band Attenuation

The large ratio between the luminosity at visible band and at the UV band can reach more than 4 orders of magnitude for *e.g.*, dM stars - the most abundant stellar objects in our local environment. Hence, a significant blocking capability at longer wavelengths is essential to obtain reliable data in the NUV band, and reduce background terms. The catadioptric nature of the optical system alleviates this requirement further, as the system PSF deteriorates significantly for  $\lambda > 300 \text{ nm}$ . We therefore set a requirement on attenuation of radiation at  $\lambda > 290 \text{ nm}$  of  $< 10^{-4}$ .

Out of band attenuation in the OTA is achieved in two steps: The use of a black mirror, and the implementation of a refractive filter in front of the detector. The former is realised by coating the spherical mirror with a custom coating of HfO and SiO<sub>2</sub> of  $\sim 30$  layers. The dielectric layers are designed such that radiation at the NUV bandpass is reflected by the mirror, while radiation at  $\lambda > 290 \text{ nm}$  is transmitted through the mirror and absorbed by the mirror substrate and in light traps on the mirror back. The mirror achieves mean attenuation levels of 1.4% for  $\lambda > 300 \text{ nm}$ , see Figure 7 left panel, and is designed, manufactured and tested by the OTA prime contractor.

The dielectric filter, located 0.55 mm in front of the focal plane array, is designed and manufactured by VIAVI Solutions. The attenuation is achieved by more than 1000 layers of Al<sub>2</sub>O<sub>3</sub>/SiO<sub>2</sub> and HfO<sub>2</sub>/SiO<sub>2</sub> coating stacks.<sup>31</sup> A significant challenge is obtaining high transmission below  $\sim 250 \text{ nm}$ . This is achieved by baking the filter at various stages in the coating process at temperatures of up to 700°C in order to fill in vacancies and imperfections at the boundaries within and between layers. Due to the high temperature required during the baking process, the filter substrate is Sapphire. In addition, the hardness of Sapphire allows us to set the filter thickness to only 4 mm while maintaining the stiffness required to resist stresses from the many layers of the coating. While Sapphire may have significant birefringence properties, this is mitigated by using Z-cut Sapphire substrate with the ordinary axis along the direction of the optical axis and placing the filter 0.55 mm in front of the detector. Measured transmission from a prototype Sapphire filter is shown in Figure 7 right panel.

### 3.3 Stray Light

The low luminosity of UV sources requires us to achieve a suppression level of  $\sim 10^{-11}$  in the visible band for out-of-field sources in order to reach our target limiting magnitude of  $> 22$  in the ULTRASAT band. While some of the suppression is achieved by the filter and mirror coating described in the previous section, a significant effort must be placed on the design of a custom baffle and vane system to reach the required level of stray light suppression. The baffle is designed in collaboration with Breault engineering (USA) with emphasis on suppression of out-of-band light from the Earth, Sun, and Moon. The two main requirements for stray light suppression are:

- Earth total scattered light flux measured on the detector (both in-band and out of band) should result in  $< 44,320 \text{ photons/cm}^2/\text{s}$ , equivalent to irradiance suppression factor of  $> 4.5 \times 10^{10}$
- Other sources (Moon, Sun diffracted by the baffle edge, etc.) should result in scattered light flux measured on the detector of  $< 10,000 \text{ photons/cm}^2/\text{s}$ . This should be taken in light of our pointing requirement of half the celestial sphere available at any given moment.

The derived baffle design is shown in Figure 5. Key features are:



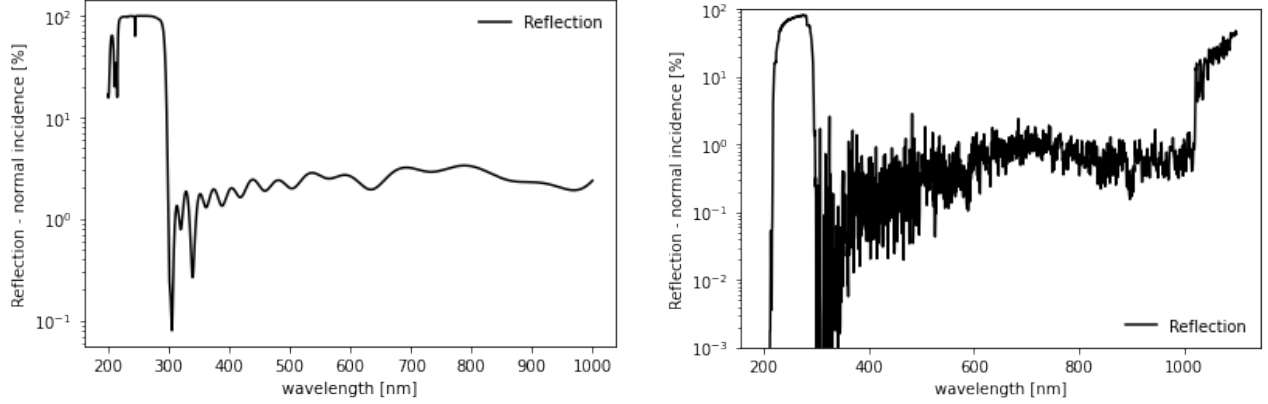


Figure 7: Left: ULTRASAT mirror reflection. Out of band attenuation of  $\sim 1.4\%$  is achieved by the mirror ; Right: ULTRASAT Sapphire filter, developed and manufactured by VIAVI Solutions, phase I measured data. We achieve more than two orders of magnitude attenuation at  $\lambda > 300$  nm, allowing us to achieve our goal requirement of  $< 10^{-4}$  attenuation. Attenuation  $> 1000$  nm is targeted in phase II.

- The baffle aperture has an angle of  $20^\circ$ , the longer side pointing towards the sun during standard observations.
- Vane angles change at the entrance of the baffle, with no vane at the baffle exit port.
- The baffle interior is coated with Acktar vacuum black to minimize reflectance from baffle walls/vanes. The vane edge thickness is the minimum that can guarantee adequate coating of the knife edge ( $\sim 200\mu\text{m}$ ).

#### 4. SUMMARY AND TIMELINE

ULTRASAT is a unique UV telescope with an exceptional large field of view dedicated for the study of the transient sky. Its unique optical design allows us to achieve mean image quality of  $\sim 10$  arcsec, while the choice of materials and its unique dielectric layer passivated sensor with custom ARC allow us to achieve efficiency of  $\sim 30\%$ . The limiting magnitude for blackbody sources with  $T > 20,000\text{K}$  is  $\sim 22.4$  for  $3 \times 300\text{sec}$  exposure, see Figure 8. Compared to previous UV missions, ULTRASAT offers a grasp 300 times larger than GALEX, the most sensitive UV satellite to date, and comparable to the upcoming Vera C. Rubin observatory. Its unique capabilities will allow us to detect EM radiation from GW sources, discover young CC-SNe during shock breakout and shock cooling phases, and determine which stellar hosts are more likely to harbor habitable planets.

UV observations hold unique challenges, and this is further enhanced in the case of ULTRASAT given its unprecedented FoV and catadioptric design. We therefore adopt several unique solutions and mitigation techniques, among them a fine-tuned baffle to suppress stray light as well as the high energy electron flux in orbit, using refractive elements from high purity materials, and the use of unique multi-layer ( $> 1000$ ) dielectric coatings to suppress out-of-band flux. Further details regarding the design, challenges and verification and test plan will be detailed in future dedicated publications.

In the past year, ULTRASAT passed the CDR stage for both the payload and bus. All critical and long lead items are now in hand or were ordered, and a payload MRR is expected to take place by the end of the year. This falls in line with the project plan to be launched during Q2/Q3 of 2025, and be fully operational during phase 5 of the large scale GW observatories.

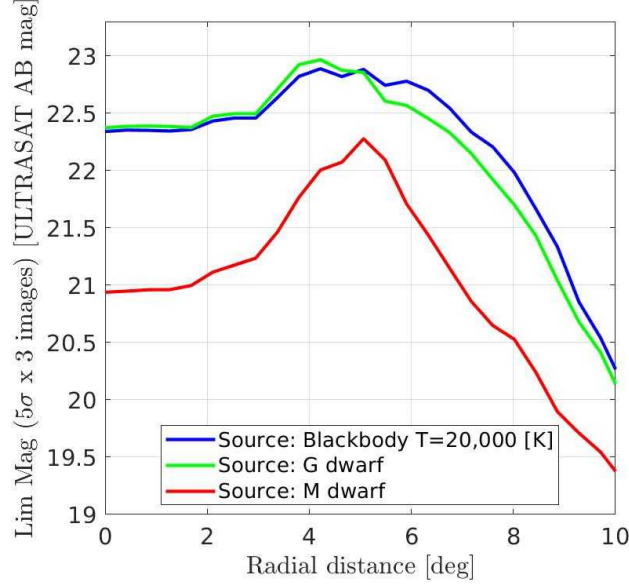


Figure 8: ULTRASAT limiting magnitude. With its unprecedented efficiency, ULTRASAT achieves an average limiting magnitude of 22.4 across a field of view of  $> 170 \text{ deg}^2$ .

## REFERENCES

- [1] Ofek, E. O. and Ben-Ami, S., “Seeing-limited Imaging Sky Surveys—Small versus Large Telescopes,” *Publications of the Astronomical Society of the Pacific* **132**, 125004 (Dec. 2020).
- [2] Ivezić, Ž., Kahn, S. M., and Tyson, J. Anthony, e. a., “LSST: From Science Drivers to Reference Design and Anticipated Data Products,” *The Astrophysical Journal* **873**, 111 (Mar. 2019).
- [3] Fernández, R. and Metzger, B. D., “Electromagnetic Signatures of Neutron Star Mergers in the Advanced LIGO Era,” *Annual Review of Nuclear and Particle Science* **66**, 23–45 (Oct. 2016).
- [4] McCully, C., Hiramatsu, D., and Howell, e. a., “The Rapid Reddening and Featureless Optical Spectra of the Optical Counterpart of GW170817, AT 2017gfo, during the First Four Days,” *The Astrophysical Journal* **848**, L32 (Oct. 2017).
- [5] Waxman, E., Ofek, E. O., Kushnir, D., and Gal-Yam, A., “Constraints on the ejecta of the GW170817 neutron star merger from its electromagnetic emission,” *Monthly Notices of the Royal Astronomical Society* **481**, 3423–3441 (Dec. 2018).
- [6] Abbott, B. P., Abbott, R., and Abbott, T. D., e. a., “Prospects for observing and localizing gravitational-wave transients with Advanced LIGO, Advanced Virgo and KAGRA,” *Living Reviews in Relativity* **21**, 3 (Apr. 2018).
- [7] Ganot, N., Gal-Yam, A., and Ofek, Eran. O., e. a., “The Detection Rate of Early UV Emission from Supernovae: A Dedicated Galex/PTF Survey and Calibrated Theoretical Estimates,” *The Astrophysical Journal* **820**, 57 (Mar. 2016).
- [8] Rabinak, I. and Waxman, E., “The Early UV/Optical Emission from Core-collapse Supernovae,” *The Astrophysical Journal* **728**, 63 (Feb. 2011).
- [9] Rubin, A. and Gal-Yam, A., “Exploring the Efficacy and Limitations of Shock-cooling Models: New Analysis of Type II Supernovae Observed by the Kepler Mission,” *The Astrophysical Journal* **848**, 8 (Oct. 2017).
- [10] Soumagnac, M. T., Ofek, E. O., and Liang, Jingyi, e. a., “Early Ultraviolet Observations of Type II In Supernovae Constrain the Asphericity of Their Circumstellar Material,” *The Astrophysical Journal* **899**, 51 (Aug. 2020).
- [11] France, K., Loyd, R. O. P., and Youngblood, Allison, e. a., “The MUSCLES Treasury Survey. I. Motivation and Overview,” *The Astrophysical Journal* **820**, 89 (Apr. 2016).

- [12] Shkolnik, E. L. and Barman, T. S., “HAZMAT. I. The Evolution of Far-UV and Near-UV Emission from Early M Stars,” *The Astronomical Journal* **148**, 64 (Oct. 2014).
- [13] Snellen, I. A. G., de Kok, R. J., le Poole, R., Brogi, M., and Birkby, J., “Finding Extraterrestrial Life Using Ground-based High-dispersion Spectroscopy,” *The Astrophysical Journal* **764**, 182 (Feb. 2013).
- [14] Ben-Ami, S., López-Morales, M., Garcia-Mejia, J., Gonzalez Abad, G., and Szentgyorgyi, A., “High-resolution Spectroscopy Using Fabry-Perot Interferometer Arrays: An Application to Searches for O<sub>2</sub> in Exoplanetary Atmospheres,” *The Astrophysical Journal* **861**, 79 (July 2018).
- [15] Stern, D., McKernan, B., and Graham, Matthew J., e. a., “A Mid-IR Selected Changing-look Quasar and Physical Scenarios for Abrupt AGN Fading,” *The Astrophysical Journal* **864**, 27 (Sept. 2018).
- [16] Edelson, R., Gelbord, J. M., and Horne, K., e. a., “Space Telescope and Optical Reverberation Mapping Project. II. Swift and HST Reverberation Mapping of the Accretion Disk of NGC 5548,” *The Astrophysical Journal* **806**, 129 (June 2015).
- [17] Kelly, B. C., Treu, T., Malkan, M., Pancoast, A., and Woo, J.-H., “Active Galactic Nucleus Black Hole Mass Estimates in the Era of Time Domain Astronomy,” *The Astrophysical Journal* **779**, 187 (Dec. 2013).
- [18] Trakhtenbrot, B., Arcavi, I., and MacLeod, Chelsea L., e. a., “1ES 1927+654: An AGN Caught Changing Look on a Timescale of Months,” *The Astrophysical Journal* **883**, 94 (Sept. 2019).
- [19] Trakhtenbrot, B., Arcavi, I., and Ricci, Claudio, e. a., “A new class of flares from accreting supermassive black holes,” *Nature Astronomy* **3**, 242–250 (Jan. 2019).
- [20] Blanchard, P. K., Nicholl, M., Berger, E., Guillochon, J., Margutti, R., Chornock, R., Alexander, K. D., Leja, J., and Drout, M. R., “PS16dtm: A Tidal Disruption Event in a Narrow-line Seyfert 1 Galaxy,” *The Astrophysical Journal* **843**, 106 (July 2017).
- [21] Kubota, A. and Done, C., “Modelling the spectral energy distribution of super-Eddington quasars,” *Monthly Notices of the Royal Astronomical Society* **489**, 524–533 (Oct. 2019).
- [22] Gezari, S., “Tidal disruptions of stars by supermassive black holes,” in [*Black Holes*], Livio, M. and Koeke-moer, A. M., eds., 286–293 (2011).
- [23] Arcavi, I., Gal-Yam, A., and Sullivan, Mark, e. a., “A Continuum of H- to He-rich Tidal Disruption Candidates With a Preference for E+A Galaxies,” *The Astrophysical Journal* **793**, 38 (Sept. 2014).
- [24] van Velzen, S., Holoien, T. W. S., Onori, F., Hung, T., and Arcavi, I., “Optical-Ultraviolet Tidal Disruption Events,” *Space Science Reviews* **216**, 124 (Oct. 2020).
- [25] Roth, N., Rossi, E. M., Krolik, J., Piran, T., Mockler, B., and Kasen, D., “Radiative Emission Mechanisms,” *Space Science Reviews* **216**, 114 (Oct. 2020).
- [26] Kochanek, C. S., “Tidal disruption event demographics,” *Monthly Notices of the Royal Astronomical Society* **461**, 371–384 (Sept. 2016).
- [27] French, K. D., Arcavi, I., and Zabludoff, A., “Tidal Disruption Events Prefer Unusual Host Galaxies,” *The Astrophysical Journal* **818**, L21 (Feb. 2016).
- [28] Wolfshmidt, G., “The development of the Schmidt telescope,” *Astronomische Nachrichten* **330**, 555 (June 2009).
- [29] Asif, A. and Barschke, M.F., e. a., “Design of the ULTRASAT UV camera,” in [*Society of Photo-Optical Instrumentation Engineers (SPIE) Conference Series*], *Society of Photo-Optical Instrumentation Engineers (SPIE) Conference Series* **11821**, 118210U (Aug. 2021).
- [30] Bastian-Querner, B., Kaipachery, N., and Küster, Daniel, e. a., “Sensor characterization for the ULTRASAT space telescope,” in [*Society of Photo-Optical Instrumentation Engineers (SPIE) Conference Series*], *Society of Photo-Optical Instrumentation Engineers (SPIE) Conference Series* **11819**, 118190F (Aug. 2021).
- [31] Ockenfus, G., “Metal-oxide Ultraviolet Narrow-band-pass Filter at 214 nm,” *Optical Interference Coatings* (2013).